Biogeosciences

EGU

Supplement of

Enhanced Southern Ocean CO_2 outgassing as a result of stronger and poleward shifted southern hemispheric westerlies

Laurie C. Menviel et al.

Correspondence to: Laurie C. Menviel (l.menviel@unsw.edu.au)

References

Landschützer, P., Gruber, N., and Bakker, D. C. E.: Decadal variations and trends of the global ocean carbon sink, Global Biogeochemical Cycles, 30, https://doi.org/10.1002/2015GB005359, 2016.

Landschützer, P., Gruber, N., and Bakker, D.: An observation-based global monthly gridded sea surface pCO2 product from 1982 onward and its monthly climatology (NCEI Accession 0160558). Version 5.5., Dataset, NOAA National Centers for Environmental Information, https://doi.org/10.7289/V5Z899N6, 2020.

Olsen, A., Key, R. M., van Heuven, S., Lauvset, S. K., Velo, A., Lin, X., Schirnick, C., Kozyr, A., Tanhua, T., Hoppema, M., Jutterstrom, S., Steinfeldt, R., Jeansson, E., Ishii, M., PÃ©rez, F. F., and Suzuki., T.: The Global Ocean Data Analysis Project version 2 (GLODAPv2) - an internally consistent data product for the world ocean, Earth System Science Data, 8, 297–323, 2016.

Sokolov, S. and Rintoul, S. R.: Circumpolar structure and distribution of the Antarctic Circumpolar Current fronts: 1. Mean circumpolar paths, Journal of Geophysical Research: Oceans, 114, https://doi.org/10.1029/2008JC005108, 2009.
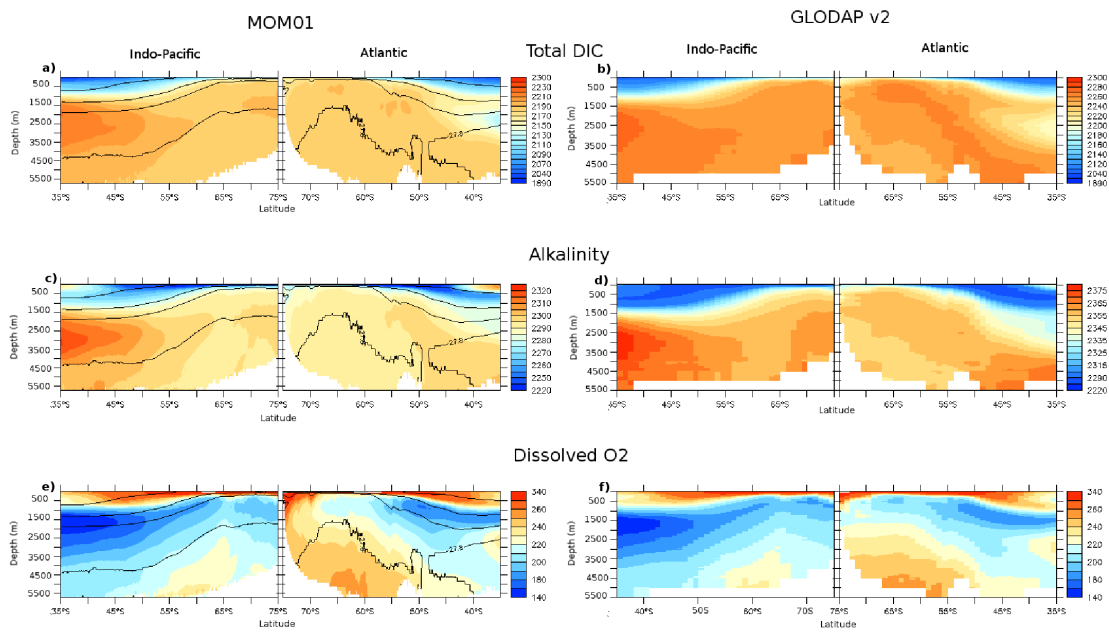
Figure S 1. Biogeochemical tracer distributions (left) as simulated in years 1990-2010 in the numerical model and compared to (right) the observed GLODAP v2 dataset (Olsen et al., 2016) for **a,b,** tDIC (μmol kg^{-1}), **c,d,** alkalinity (μmol kg^{-1}), and **e,f,** dissolved oxygen (μmol kg^{-1}), zonally averaged over the Indo-Pacific and Atlantic basins. The density of the AABW ($\geq$1028.31 kg/m^3), the AAIW (1027.5$\leq$AAIW$\leq$1026.95 kg/m^3) and the SAMW ($\leq$1026.95 kg/m^3) are overlaid. The core of Pacific Deep Water (PDW, 1027.7 kg/m^3) and North Atlantic Deep Water (NADW, 1027.75 kg/m^3) are also overlaid in the Indo-Pacific and Atlantic sectors respectively.
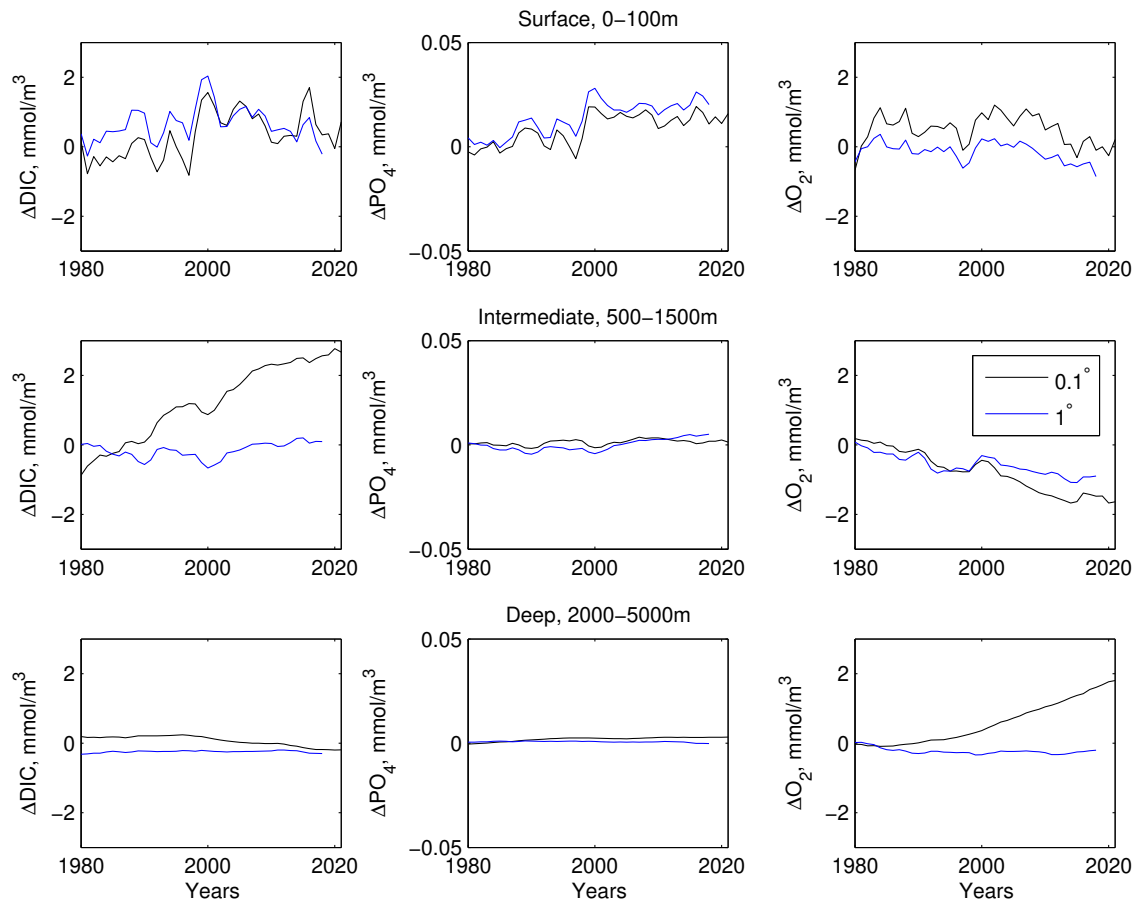
Figure S 2. Biogeochemical tracers time-series averaged over the Southern Ocean (35°S-75°S) in the ACCESS-OM2-01 (black) and ACCESS-OM2 (blue) models. From left to right: nDIC, PO$_4$ and O$_2$ averaged over (top) the top 100m, (middle) between 500-1500m and (bottom) below 2000m depth.
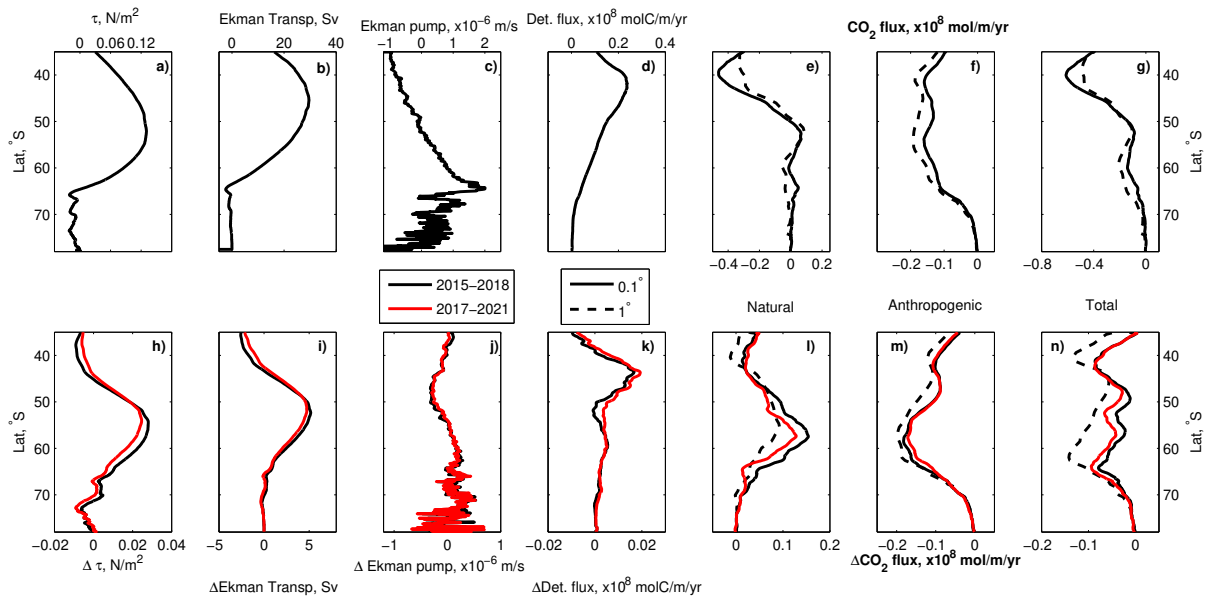
Figure S 3. Zonally averaged (a,h) windstress (N/m^2), (b,i) Ekman transport (Sv, positive is northward), (c,j) Ekman pumping (m/s, positive is upward), and zonally integrated (d,k) detritus flux at 100m depth (x10^8 molC/m/yr), (e,l) natural, (f,m) anthropogenic and (g,n) total ocean to atmospheric CO_2 flux (molC/m/yr) for (top) years 1980-1982 and (bottom) anomalies for years 2015-2018 (black) and years 2017-2021 (red) compared to years 1980-1982. Results of ACCESS-OM2-01 are in solid lines and of ACCESS-OM2 in dashed lines.
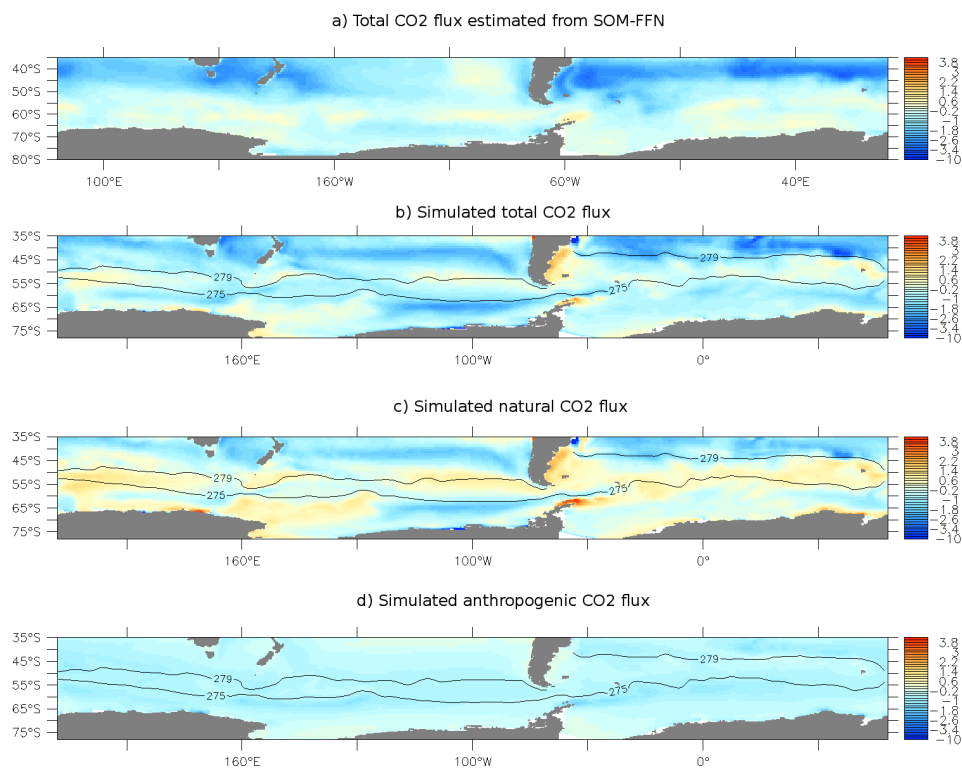
Figure S 4. a) Total ocean to atmosphere CO_2 flux (molC/m^2/yr) as estimated from the SOM-FFN for the period 1982-2021 (Landschützer et al., 2016, 2020). Simulated b) Total, c) natural and d) anthropogenic ocean to atmosphere CO_2 flux (molC/m^2/yr) averaged over the period 1982-2018 of the 1° resolution simulation (ACCESS-OM2). The black contours indicate (from south to north) the northern edges of the PF and SAF using the definition of Sokolov and Rintoul (2009).
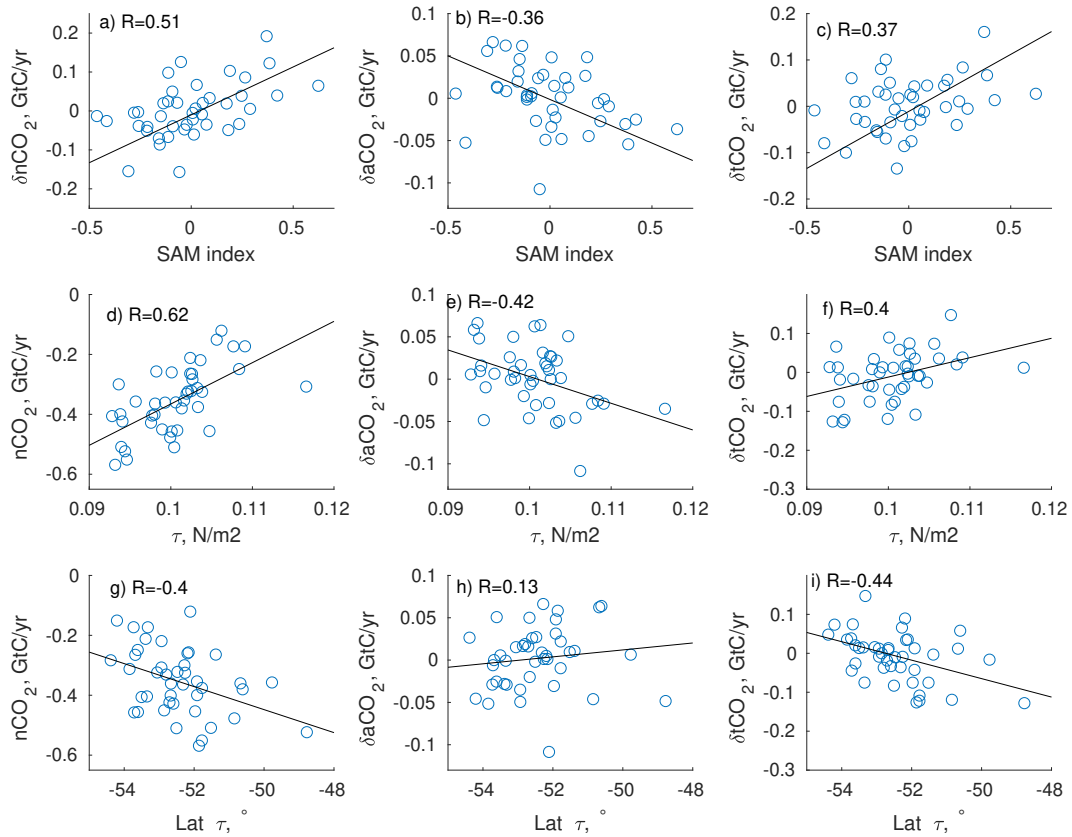
Figure S 5. Scatter plots of annual mean SO a) detrended nCO_2, b) detrended aCO_2 and c) detrended tCO_2 versus detrended SAM. d) nCO_2 versus SO zonal mean windstress; e-f) same as c for detrended aCO_2 and tCO_2, respectively. g) nCO_2 versus latitude of the maximum windstress; h,i) same as g for detrended aCO_2 and tCO_2, respectively. Black lines indicate the linear fit, and R, the correlation coefficient. The SAM index is calculated from JRA55-do dataset.
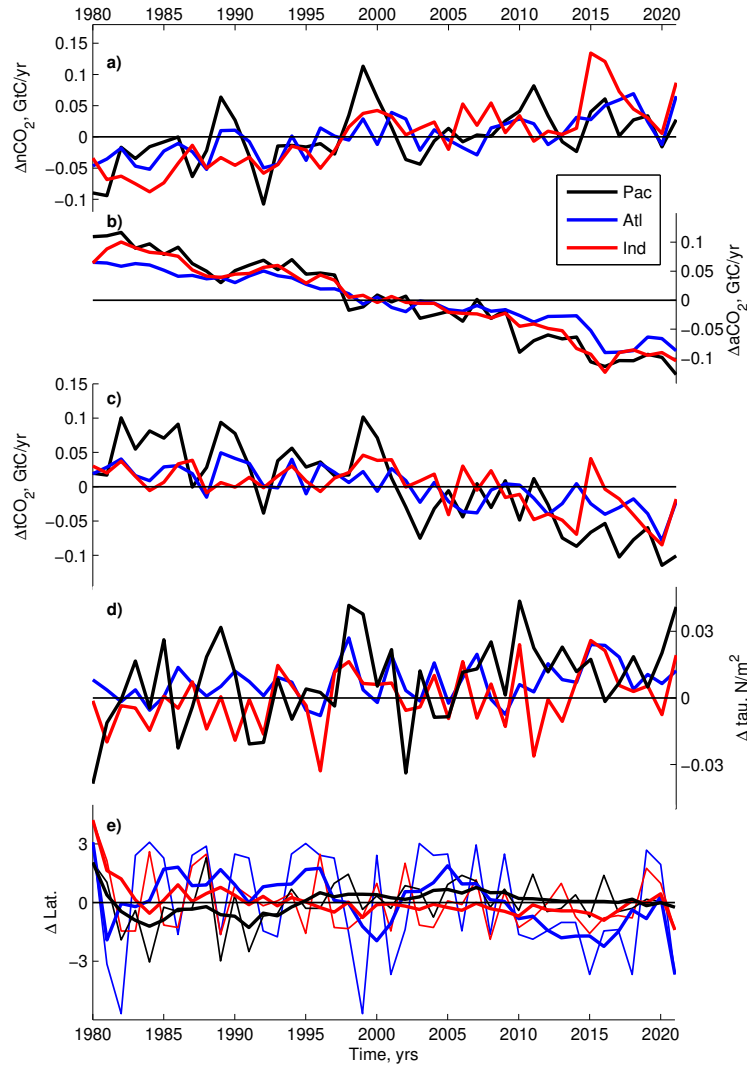
Figure S 6. Time-series of a) nCO_2, b) aCO_2 and c) tCO_2 ocean to atmosphere flux anomalies (GtC/yr) compared to the 1980-2021 mean and integrated over the (blue) Atlantic, (red) Indian and (black) Pacific sectors of the Southern Ocean (south of $35°$S). d) Maximum windstress anomaly (N/m^2) and e) change in latitude ($°$, poleward is negative) of the maximum windstress over each sector of the SO compared to the 1980-2021 mean. In e) thin lines represent annual means while thick lines represent 5-yr running means.
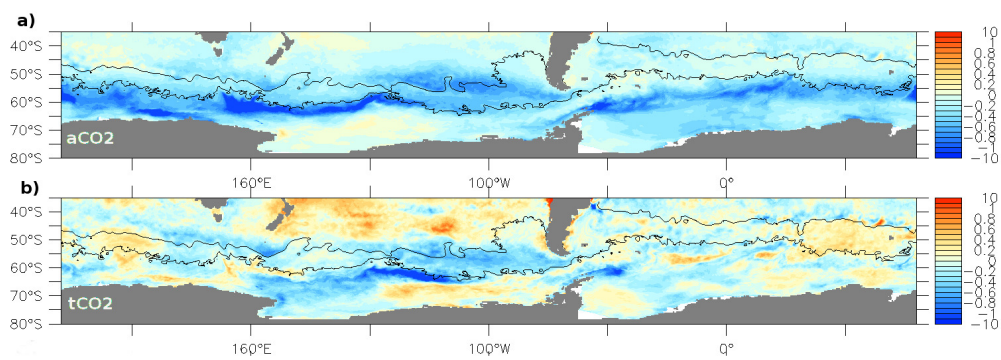
Figure S 7. a) aCO$_2$ and b) tCO$_2$ flux (mol/m^2/yr) anomalies for a composite of positive phases of the SAM ($\geq$0.83, i.e. 1998, 1999, 2010, 2015 and 2021) compared to a composite of negative SAM years (1980, 1991, 1992, 2002).
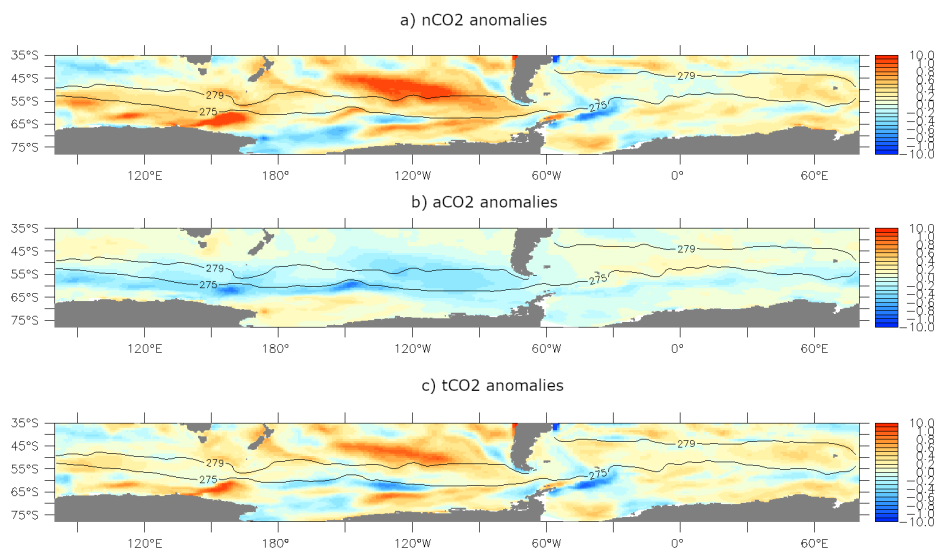
Figure S 8. Simulated a) natural, b) anthropogenic and c) total ocean to atmosphere CO_2 flux anomalies (molC/m^2/yr) for the positive SAM (1998, 1999, 2010, 2015) composite compared to the negative SAM (1980, 1991, 1992, 2002) composite in the 1° resolution simulation (ACCESS-OM2). The simulated aCO_2 and tCO_2 fields include a correction for the fact that the SAM positive composite represents more recent years than the negative SAM composite. The black contours indicate (from south to north) the northern edges of the PF and SAF using the definition of Sokolov and Rintoul (2009).